Organic & Biomolecular Chemistry

PAPER

View Article Online
View Journal

Cite this: DOI: 10.1039/c5ob01445j

Importance of topology for glycocluster binding to *Pseudomonas aeruginosa* and *Burkholderia ambifaria* bacterial lectins†

Caroline Ligeour,[a] Lucie Dupin,[b] Anthony Angeli,[a] Gérard Vergoten,[d] Sébastien Vidal,[c] Albert Meyer,[a] Eliane Souteyrand,[b] Jean-Jacques Vasseur,[a] Yann Chevolot*[b] and François Morvan*[a]

Received 15th July 2015,
Accepted 18th September 2015

DOI: 10.1039/c5ob01445j

www.rsc.org/obc

Pseudomonas aeruginosa (PA) and *Burkholderia ambifaria* (BA) are two opportunistic Gram negative bacteria and major infectious agents involved in lung infection of cystic fibrosis patients. Both bacteria can develop resistance to conventional antibiotherapies. An alternative strategy consists of targeting virulence factors in particular lectins with high affinity ligands such as multivalent glycoclusters. LecA (PA-IL) and LecB (PA-IIL) are two tetravalent lectins from PA that recognise galactose and fucose respectively. BambL lectin from BA is trimeric with 2 binding sites per monomer and is also specific for fucose. These three lectins are potential therapeutic targets in an anti-adhesive anti-bacterial approach. Herein, we report the synthesis of 18 oligonucleotide pentofuranose-centered or mannitol-centered glycoclusters leading to tri-, penta- or decavalent clusters with different topologies. The linker arm length between the core and the carbohydrate epitope was also varied leading to 9 galactoclusters targeting LecA and 9 fucoclusters targeting both LecB and BambL. Their dissociation constants (K_d) were determined using a DNA-based carbohydrate microarray technology. The trivalent xylo-centered galactocluster and the ribo-centered fucocluster exhibited the best affinity for LecA and LecB respectively while the mannitol-centered decafucocluster displayed the best affinity to BambL. These data demonstrated that the topology and nature of linkers were the predominant factors for achieving high affinity rather than valency.

Introduction

Pseudomonas aeruginosa (PA) and *Burkholderia ambifaria* (BA) are opportunistic pathogens involved in nosocomial diseases and they especially affect cystic fibrosis patients. PA has two soluble lectins LecA and LecB involved in its virulence.[1] Both lectins are homotetrameric with one binding site per monomer and one or two calcium ions involved in the binding site respectively. LecA is galactose specific with an association constant (K_a) of 3.4×10^4 M^{-1} while LecB is fucose specific with a K_a of 1.6×10^6 M^{-1}. LecA has a cobblestone shape where the binding sites are located at the corner of the rectangle (32 and 70 Å away on the width and length, respectively).[2,3] Due to this configuration, several studies suggest that galactoclusters can reach simultaneously two binding sites along the small side of one tetramer leading to a glycoside cluster effect.[3,4] LecB has more or less a tetrahedral spatial distribution of the binding sites that are more difficult to reach simultaneously and very few glycoside cluster effects have been reported so far with LecB.[5,6] Furthermore, its affinity for monovalent fucose is already high with a K_d in the micromolar range.[1,2]

BA expresses a fucose-binding lectin called BambL. Similarly to LecB, it has a very high affinity for fucose (a K_d of 0.96 μM).[7] It is a crown shaped trimeric lectin with two binding sites per monomer. The six binding sites are on the same side of the protein with a inter binding site distance ranking between 18 and 36 Å. So far very little fucoclusters targeting BambL have been synthesized and no glycoside cluster effect has been reported.[8,9] Nevertheless, its topology is favor-

[a]*Institut des Biomolécules Max Mousseron (IBMM), UMR 5247 CNRS, Université de Montpellier, ENSCM, place Eugène Bataillon, CC1704, 34095 Montpellier Cedex 5, France. E-mail: morvan@univ-montp2.fr*
[b]*Université de Lyon, Institut des Nanotechnologies de Lyon UMR CNRS 5270, Ecole Centrale de Lyon, 36 avenue Guy de Collongue, 69134 Ecully, France. E-mail: yann.chevolot@ec-lyon.fr*
[c]*Institut de Chimie et Biochimie Moléculaires et Supramoléculaires (ICBMS), Laboratoire de Chimie Organique 2 – Glycochimie, UMR 5246, CNRS, Université Claude Bernard Lyon 1, 43 Boulevard du 11 Novembre 1918, 69622 Villeurbanne, France*
[d]*Unité de Glycobiologie Structurelle et Fonctionnelle (UGSF), UMR 8576 Université de Lille 1, Cité Scientifique Avenue Mendeleiev, Bat C9, 59655 Villeneuve d'Ascq cedex, France*

†Electronic supplementary information (ESI) available: NMR data and HPLC of glycoclusters. See DOI: 10.1039/c5ob01445j

able to the glycoside cluster effect with binding sites that can be reached by multivalent ligands with a topology in close relationship with the AB_5 shiga toxin complexes.

The use of glycoclusters exhibiting high affinity for the targeted lectins has emerged as a promising strategy to fight against such pathogens.[5,10] Since there is no pressure on the bacteria this strategy should not induce a resistance phenomenon. However, the design of good candidates remains empirical since the precise mode of recognition of multivalent glycoclusters by their bacterial lectin partners is still not fully understood.

Results and discussion

We have previously reported the syntheses of glycoclusters with a hexose-platform exhibiting either galactose[11–13] or fucose[12,14] epitopes for interactions with LecA and LecB respectively. To gain more insight into the effect of topology and valency on the affinity of the corresponding glycoclusters toward LecA and LecB, we have designed two new families of glycoclusters. The first one used furanose-based platforms such as arabinose, ribose and xylose (**3a–c**, Fig. 1) and the second one used an acyclic azido-mannitol (**10**, Fig. 1). The furanose platforms exhibit three hydroxyl functions which are differently orientated in the space according to the nature of the furanose to study the effect of the orientation of the 2′- and 3′-hydroxyl groups of the furanose moiety. The mannitol core **10** exhibits five hydroxyl functions on a flexible linear scaffold. The impact of rigidity and multivalence on the affinity for LecA and LecB can therefore be evaluated using these different scaffolds. The affinity of the fucoclusters toward BambL was also evaluated since this lectin from *Burkholderia ambifaria* recognizes fucose moieties.

According to our strategy, the polyhydroxylated platforms **3a–c** and **10** were immobilized on a solid support and each hydroxyl was phosphitylated using phosphoramidite chemistry with an alkyne linker leading to scaffolds bearing three or five alkynes. In addition, two alkyne functions were introduced on each hydroxyl of the reduced mannosyl platform leading to a decaalkyne scaffold. Then, the conjugation between the polyalkyne scaffolds and the carbohydrate azides (galactoside **16** or fucoside **17**) occurred through copper-catalyzed azide–alkyne cycloaddition (CuAAC) affording the expected glycoclusters exhibiting from three to ten galactose or fucose residues. Finally, a DNA sequence was incorporated for immobilization on a DNA microarray of the final glycocluster leading to a glycoarray. K_d values of the glycoclusters toward LecA, LecB or BambL were determined using this glycoarray.

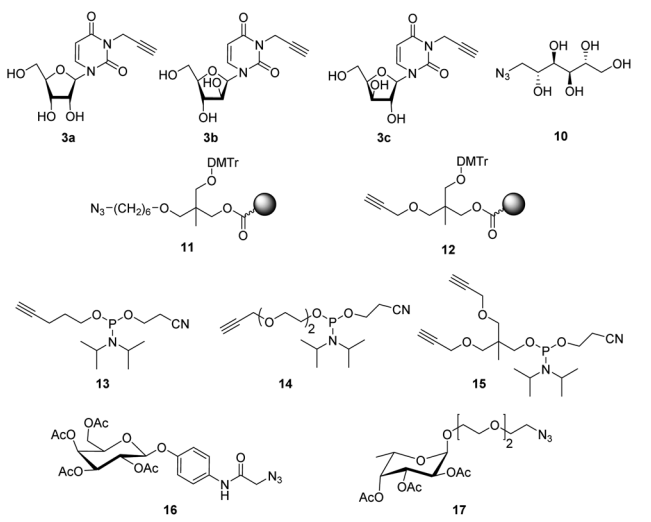

Fig. 1 Structure of building blocks used for the synthesis of the glycoclusters.

Building block synthesis

The different building blocks required for their further assembly to obtain the desired glycoclusters were synthesized: the three ribo, arabino and xylo-furanoside propargyl platforms **3a–c**, the 6-azido-6-deoxymannitol **10**, azide **11**[15] and alkyne **12**[16] solid supports, three different alkyne phosphoramidites exhibiting one **13**[15] and **14**[12] or two **15**[17] alkynes and β-D-galactoside **16**[18] or α-L-fucoside **17**[19] azide derivatives (Fig. 1).

For the synthesis of the three different furanose scaffolds, we used ribo-, arabino- and xylo-furanosyl uracil since it is easy to introduce an alkyne function on the N^3 of uracil by selective alkylation.[20] Commercially available ribo-**1** and arabino-**2** uracils were treated with propargyl bromide and potassium carbonate in DMF at 60 °C overnight to give compounds **3a** and **3b** respectively exhibiting N^3-propargyl for subsequent immobilization on the azide solid support **11** (Scheme 1). Since xylo-furanosyl uracil is not commercial, N^3-propargyl xylo-furanosyl uracil **3c** was synthesized in two steps by glycosylation of the 1,2,3,5-tetra-*O*-acetyl-D-xylofuranose with uracil, using bis(trimethylsilyl)acetamide and trimethylsilyl trifluoromethanesulfonate in acetonitrile. In accord with Baker's rule,[21] the direct condensation of the suitably protected 2′-*O*-acyl-D-xylofuranose **4** and uracil led to the formation of β (*trans*-1′,2′) nucleoside **5**. The resulting peracetyl xylouracil

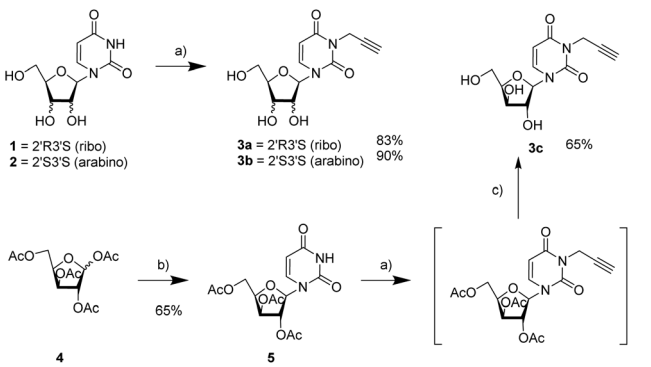

Scheme 1 Synthesis of ribo-, arabino- and xylo-furanosyl uracils **3a–c**. (a) $BrCH_2CCH$, K_2CO_3, DMF, 60 °C, overnight; (b) *N*,*O*-Bis(trimethylsilyl) acetamide, TMSOTf, CH_3CN, reflux, 4 h 30 min; (c) MeOH, rt.

5 was alkylated as described above. The deprotection of the acetyl groups on the xylofuranoside was achieved by addition of methanol in the basic medium to give **3c**.

The linear platform **10** was obtained from methyl α-D-mannopyranoside **6** (Scheme 2). The primary 6-hydroxyl group was selectively tosylated in pyridine. Then, the tosyl group was replaced by an azide function by treatment with NaN_3 to afford **8**.[22] Acetal **8** was converted to the corresponding hemiacetal **9** under acidic conditions and reduction using sodium borohydride[23] afforded 6-azido-6-deoxy-D-mannitol **10**.

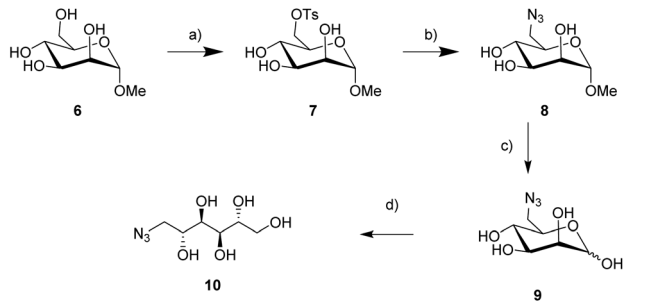

Scheme 2 Synthesis of 6-azido-6-deoxymannitol **10**. (a) TsCl, pyridine, 22 h, 0 °C, 65%; (b) NaN_3, DMF, 2 h, 80 °C, 84%; (c) HCl, H_2O, dioxane, 2 h, reflux, 46%; (d) $NaBH_4$, EtOH, 1 h, rt, 82%.

Synthesis of glycocluster oligonucleotide conjugates

Ribo-, arabino-, xylo-furanosyl uracil-centered glycol-oligonucleotides were synthesized using the building blocks reported in Fig. 1. The first step was the immobilization of scaffolds **3a–c** on azide solid support **11** by CuAAC under microwave assistance (Scheme 3). The resulting tri-hydroxyl scaffolds **18a–c** were then phosphorylated with alkyne phosphoramidites **13** or **14** using a DNA synthesizer with a triple coupling step. Then, the oligonucleotide was elongated and labelled with a fluorescent dye (Cy3) using phosphoramidite chemistry. The resulting trialkyl furanoside oligonucleotide conjugates **19a–c** and **20a–c** were deprotected and released from the solid support by ammonia treatment leading to the trialkyl furanoside oligonucleotide conjugates **21a–c** and **22a–c** exhibiting different furanoside scaffolds (*i.e.* ribo-, arabino- or xylo) with alkyne linkers of different lengths (pent-4-ynyl phosphodiester **21** or propargyl diethyleneglycyl phosphodiester **22**) in solution. Crude materials were analyzed and characterized by HPLC and MALDI-TOF spectrometry. Around 100 nmol of crude material was conjugated with either galactoside **16** or fucoside **17** azide by CuAAC using copper nanopowder[24] under

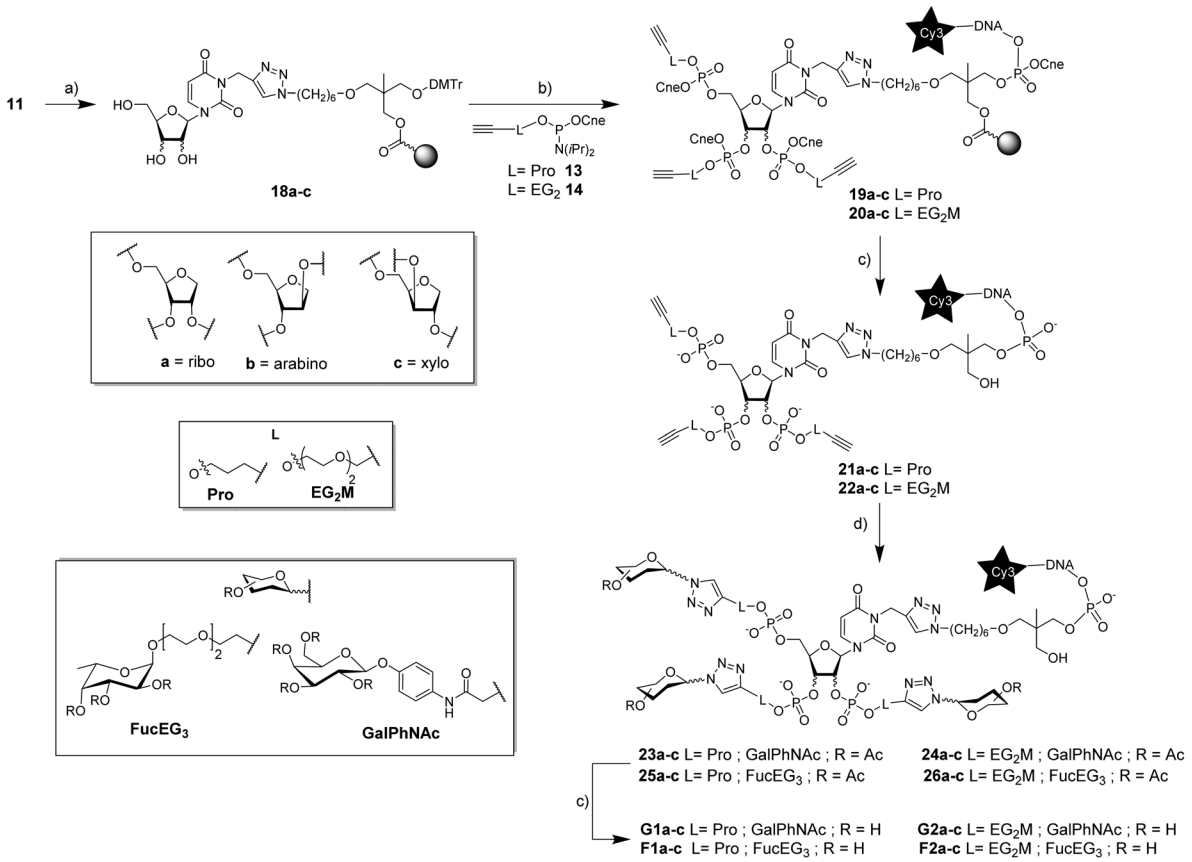

Scheme 3 Synthesis of the triglycocluster oligonucleotides **G1a–c**, **G2a–c**, **F1a–c** and **F2a–c**. (a) **3a–c**, $CuSO_4$, Na ascorbate, MeOH/H_2O (1 : 1), MW, 60 °C, 1 h; (b) Solid Phase Oligonucleotide Synthesis (SPOS) with **13** or **14**, then SPOS with A, T, C, G, Cy3; (c) NH_4OH; (d) Cu^0, **16** or **17**.

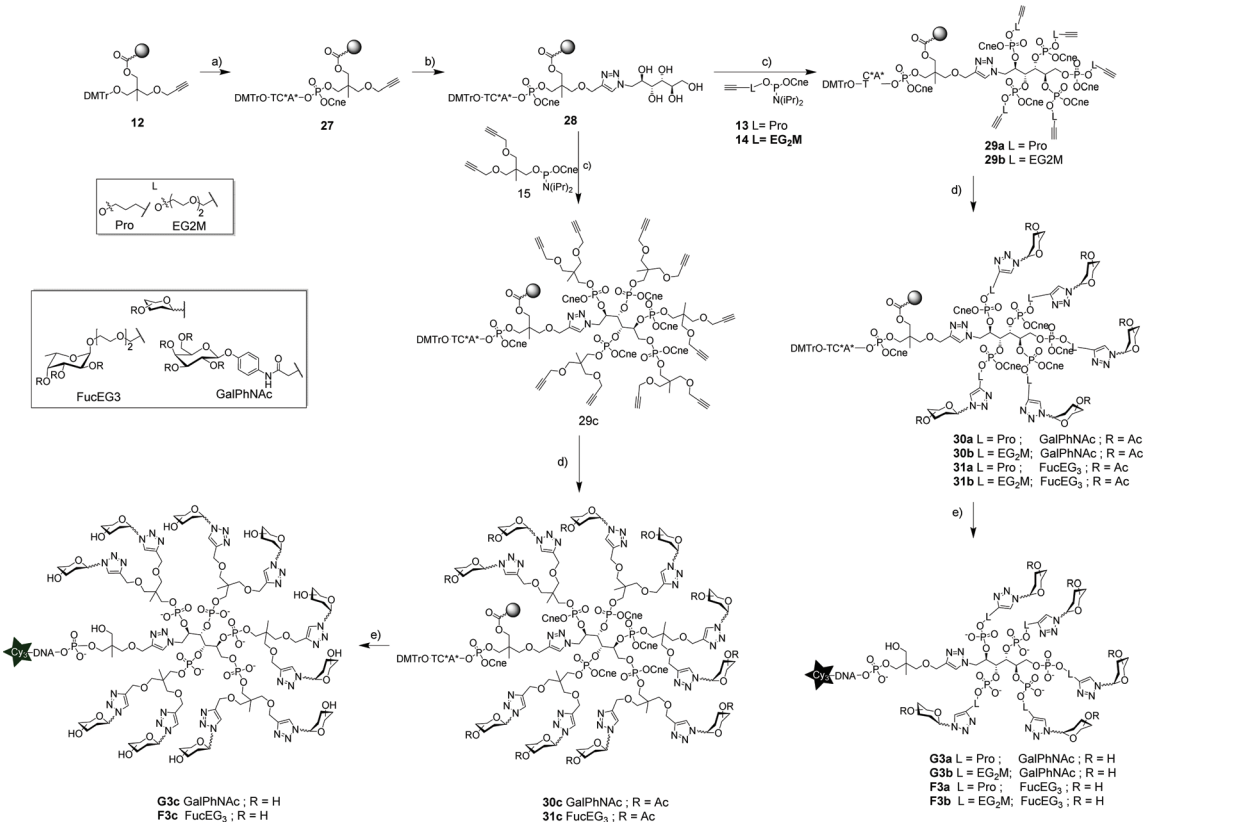

Scheme 4 Synthesis of the penta- and deca-glycocluster oligonucleotides **G3a–c** and **F3a–c**. (a) SPOS with A, T, C; (b) **10**, $CuSO_4$, Na ascorbate, MeOH/H_2O (1 : 1), MW, 65 °C, 1 h; (c) SPOS with 3; (d) **16** or **17**, $CuSO_4$, Na ascorbate, dioxane/H_2O (1 : 1), MW, 70 °C, 1 h; (e) SPOS with A, T, C, G, Cy3, (ii) NH_4OH.

microwave assistance. Finally, a short ammonia treatment was applied to remove the acetyl groups. The twelve resulting glycoclusters exhibiting three galactosides (**G1a–c** and **G2a–c**) or three fucosides (**F1a–c** and **F2a–c**) with different scaffolds (ribo-, arabino- and xylo-furanose) and with short (pro, **G1**) or long (EG_2M, **G2**) linkers were purified by C_{18} HPLC.

For the mannitol-centered oligonucleotides, the synthetic strategy was changed since difficulties in characterizing the final glycocluster oligonucleotide conjugates were encountered due to their high molecular weights. A short DNA sequence was synthesized on the alkyne solid support **12** and then the mannitol azide **10** was immobilized by CuAAC with copper sulfate and sodium ascorbate under microwave assistance (Scheme 4). The resulting pentahydroxyl compound **28** was phosphorylated with the three different phosphoramidites **11–13** with a triple coupling step to obtain respectively **29a–c**. Both galactoside and fucoside azide derivatives were conjugated on a solid support by CuAAC using $CuSO_4$ and sodium ascorbate to afford **30a–c** and **31a–c** respectively. A few beads were withdrawn and treated with ammonia for deprotection and release. After evaporation, the sample was analyzed by HPLC and MALDI-TOF showing the efficient introduction of carbohydrate moieties on the polyalkyne scaffolds. Then, the remaining oligonucleotide was elongated and labeled with Cy3. A final treatment with ammonia led to four pentaglycoclusters **G3a–b**, **F3a–b** and two decaglycoclusters **G3c**, **F3c**.

The affinity (K_d) of the eighteen new glycoclusters displaying 3, 5 or 10 galactose or fucose moieties with different topologies and conjugated to different DNA sequences (Table S1†) was determined by using a microarray (Table 1). The 9 galactoclusters can only target LecA while the 9 fucoclusters can target both LecB and BambL. The microarray was elaborated by DNA Directed Immobilization (DDI).[26,27] Each glycocluster labelled with Cy3 and bearing a specific DNA sequence was hybridized specifically with an immobilized complementary DNA sequence on the array.[28,29] Fluorescence scanning of the Cy3 signal allows verifying glycocluster immobilization with a deviation lower than 14% illustrating similar surface densities for all immobilized glycoclusters. Microstructured glass slides, bearing 40 microwells, were used as an array of 64 spots/microwell allowing 40 independent experiments on one single slide. In each microwell, two glycoclusters to be tested were immobilized and incubated with increasing concentrations (one concentration per well) of Alexa-647-labelled lectin (LecA, LecB or BambL). Scanning at 635 nm provided the binding isotherms for each glycocluster/lectin binding event. K_d values were obtained using the linear regression described in the Experimental section.[30] The background noise of the Alexa-647 fluo-

Table 1 K_d values of the DNA-glycoclusters towards LecA, LecB or BambL determined by using a DNA directed immobilization glycoarray[25]

		K_d (nM)		
Glyco-[a]	Clusters	LecA	LecB	BambL
G1a	RiboPro	66	—	—
G2a	RiboEG_2M	54	—	—
G1b	AraPro	64	—	—
G2b	AraEG_2M	62	—	—
G1c	XyloPro	54	—	—
G2c	XyloEG_2M	49	—	—
G3a	Mannipro	66	—	—
G3b	ManniEG_2M	78	—	—
G3c	Manni2	50	—	—
F1a	RiboPro	—	56	20.1
F2a	RiboEG_2M	—	73	21.2
F1b	AraPro	—	81	25.1
F2b	AraEG_2M	—	76	29.6
F1c	XyloPro	—	62	20.5
F2c	XyloEG_2M	—	93	26.5
F3a	ManniPro	—	91	22.8
F3b	ManniEG_2M	—	95	18.2
F3c	Manni2	—	84	13.8

[a] Name of the core (ribose, arabinose, xylose or mannitol) with the nature of linker L (Pro or EG_2M) and manni2 for mannitol with two glycosides per hydroxyl.

rescence signal was very low (below 20 a.u.) illustrating that Alexa-647-labelled lectin was not adsorbed nonspecifically on the surface.

The 9 galactoclusters tested exhibited the same order of magnitude of binding strength with K_d values between 49 and 78 nM for LecA. For each trimeric cluster, the hydrophilic and flexible EG_2M linker (**G2a–c**) seems to be slightly preferred to the short hydrophobic Pro linker (**G1a–c**) especially for the ribose core. The opposite was observed for the mannitol core (**G3a** *vs.* **G3b**). It was previously observed that the length of a linker could have a strong effect on binding. Thus dimeric galactoclusters with a linker differing from only four methylenes exhibit a four-fold difference of binding.[31]

Regardless of the linker or the valence (3 or 5), the xylose core seems to be preferred. Then, with a slightly lower affinity, arabinose and ribose scaffolds showed comparable binding properties. The decavalent glycocluster **G3c** displayed a similar K_d value (50 nM) than the best trimeric glycocluster **G2c** (49 nM). These data could be explained by some steric hindrances leading to a lower accessibility of the ten galactoside motifs. Furthermore, we have previously observed that mannose-centered galactoclusters exhibiting four phenyl galactoside motifs with Pro and EG_2M linkers have a K_d value of 57 and 39 nM[32] respectively, showing also the benefit of a longer linker. Thus, the affinity of the xylose centered trigalactocluster **G2c** to the EG_2M linker exhibiting a K_d value of 49 nM is not so different, taking into account that only three motifs are involved in the construct.

These data showed that the "aromatic effect" has a strong consequence on the high binding of glycoclusters, as already observed by others and us.[13,32–38] Nevertheless, the topology brings an additional benefit allowing high binding with only trivalent clusters.

In the case of LecB, glycoclusters with ribo and xylo cores exhibited the best affinities (56 and 62 nM). A stronger affinity was found with the shortest Pro linker (**F1a** and **F1c**) than with the EG_2M linker (**F2a** and **F2c**). Surprisingly, for the glycoclusters with an arabinose core (**F1b–F2b**) or with the mannitol core (**F3a–F3b**), the effect of the linker on the binding was not significant. Interestingly, the glycoclusters with an arabinose core were less prone to bind LecB. Finally the decavalent cluster (**F3c**) bound LecB better than the pentavalent clusters but lower than the trivalent clusters. One can imagine that the rigidity of the furanose cores has an entropic benefit in the interaction of the corresponding clusters leading to better binding.

For BambL, all fucoclusters displayed strong binding with only a few differences between them (K_d from 13.8 to 29.6 nM). The increase of the length of the linker from Pro to EG_2M was slightly detrimental for the furanose cores in contrast to the mannitol ones. Ribo and xylo-centered clusters were found to be better ligands toward BambL than toward arabino-centered ones. Interestingly, the decafucocluster (**F3c**) displayed the strongest affinity (K_d = 13.8 nM) and this effect can be explained by the fact that the CRDs of BambL are localized on the same side leading to easy and simultaneous (multivalent) access to several fucoses of the cluster in a "glycoside cluster effect" fashion.

In order to understand why glycoclusters with an arabinofuranose core have a higher dissociation constant (K_d) against LecA and LecB compared to ribofuranose and xylofuranose, preliminary molecular modeling studies have been performed. For each lectin, the glycoclusters exhibiting the best affinity have been chosen: **G2a**, **G2b G2c** and **F1a**, **F1b F1c**. Quantum semi empirical calculations using the PM6 Hamiltonian[39] and the solvation model SM5.4/A[40] showed that β-D-ribofuranose, β-D-arabinofuranose and β-D-xylofuranose exhibit a very similar heat of formation both under vacuum (ΔH_f) and in aqueous solution (ΔH_{aq}) (Table 2). From a structural point of view, the main differences among the three sugars lie in the chiralities of carbon 2 and carbon 3 of the furanose ring (Table 2) while that of carbons 1 and 4 is the same (R).

According to these findings, the differences in glycocluster interactions with LecA and LecB are supposed to be related to branches originating from C2 and C3. Accordingly, *in silico* molecular modelling was performed and the following empirical potential energies of interaction were obtained (Table 3). They clearly show that arabinofuranose derivatives (**G2b** and **F1b**) are the weakest ligands as found from their K_d values. When docking was applied with the epitopes on carbons 4 and 2 involved in the CRD, the empirical potential energies of interaction (ΔE) were not in agreement with the K_d values. These data strongly suggest that the interaction with lectin occurred with epitopes on carbons C2 and C3.

In the case of LecA interaction, the difference of the energies of interaction could be tentatively explained by the position of the galactose with the linker on carbon 4 that brought

Table 2 ΔH_f and ΔH_{aq} and absolute configuration of carbon 2 and 3 obtained by quantum semi empirical calculations using PM6 Hamiltonian and SM5.4/A solvation model

Furanose	ΔH_f, kcal mol^{-1}	ΔH_{aq}, kcal mol^{-1}	Absolute configuration	
			C2	C3
β-D-Ribo	−231.8	−252.0	R	S
β-D-Arabino	−230.9	−251.2	S	S
β-D-Xylo	−229.7	−251.9	R	R

Table 3 Empirical potential energy of interaction (ΔE) and experimental dissociation constants (K_d)

Complex	ΔE (kcal mol^{-1})	K_d (nM)
LecA–**G2a**	−255.8	54
LecA–**G2b**	−198.9	62
LecA–**G2c**	−244.4	49
LecB–**F1a**	−232.7	56
LecB–**F1b**	−192.0	81
LecB–**F1c**	−222.0	62

an additional stabilization by interaction with the lectin. For LecA–**G2a**, the free ending galactose interacts with the R48 residue of LecA. In the case of LecA–**G2c** (Fig. 2a), the interaction takes place with P38 and T39 (Fig. 2b). Finally for LecA–**G2b**, no interaction occurs (Fig. 2c).

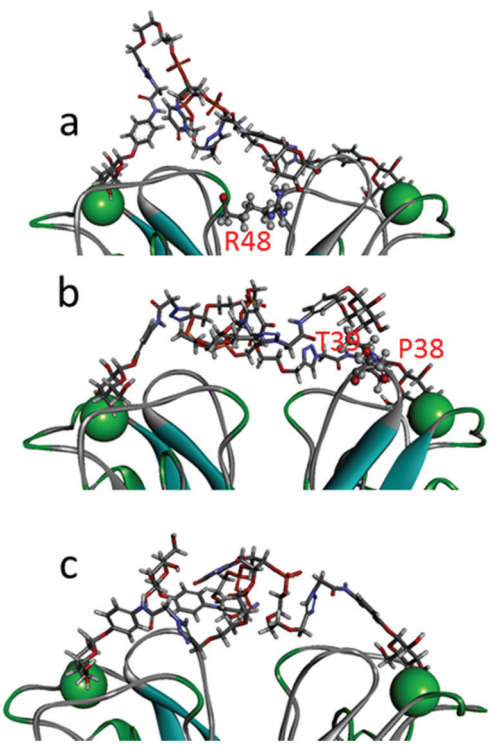

Fig. 2 LecA in complex with (a) **G2a**, (b) **G2c** and (c) **G2b**.

The situation of LecB is slightly different. In the case of **F1a** and **F1c**, the free fucose, on the C4 branch, is located at an equal distance from the two binding sites. **F1a** (Fig. 3a) exhibits strong intramolecular hydrogen bonds, a pseudo stacking interaction with the uracil ring and some interactions with residues A1, Q3 and L76. The free fucose in **F1c** (Fig. 3b) also takes a central position and hence displays strong interactions with N34, K62 and Q64. In the case of **F1b**, the free fucose is oriented towards the triazole moiety of branch on C2 leading to some interactions with P73 and S74 (Fig. 3c).

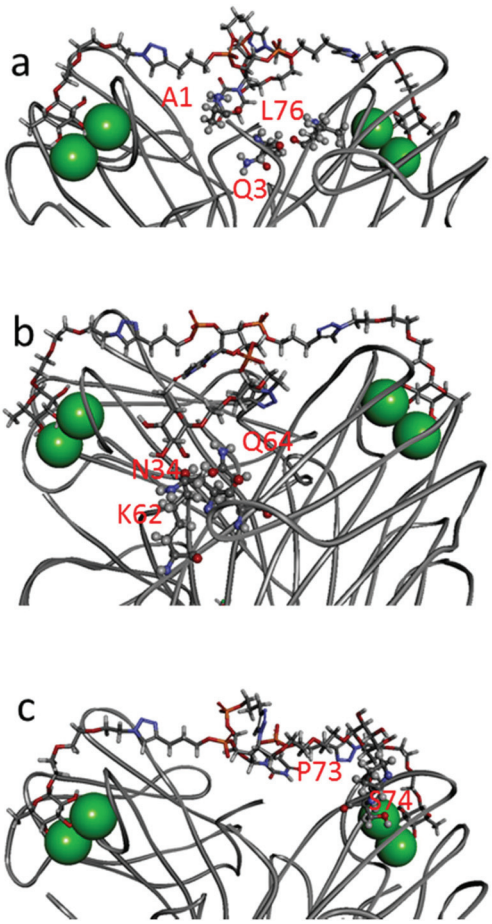

Fig. 3 LecB in complex with (a) **F1a**, (b) **F1c** and (c) **F1b**.

Conclusion

In the present report, 18 glycoclusters were synthesized in order to target two lectins of PA (LecA and LecB) and one lectin from BA (BambL). These three lectins are virulence factors involved in the adhesion and/or in biofilm formation. Their binding to the 18 glycoclusters was evaluated using the DDI-based glycocluster array allowing for the determination of their K_d values which were below 100 nM. An *in silico* molecular modeling study suggested that, for furanose-centered glycoclusters, epitopes borne on carbons 2 and 3 are involved in the CRD of LecA or LecB while the free epitope on carbon 4 for ribose and xylose interacts with the lectin leading to an additional stabilization. The topology and nature of linkers were the predominant factors for achieving high affinity rather than valency. LecB and BambL showed different bonding profiles toward the set of 9 fucosylated clusters suggesting that the topology of the binding sites leads to an additional (additional with respect to the saccharide residues) selectivity toward the cluster structure (topology and linker). These selectivity profiles can be viewed as a fingerprint of the lectin. These results demonstrated that high avidity of a glycocluster to a lectin is a delicate fine-tuning of its topology.

Experimental

General methods

All reagents for synthesis were commercial and used without further purification. Solvents were commercial and used without further purification. All moisture sensitive reactions were performed under an argon atmosphere. NMR solvents were purchased from Euriso-Top. NMR spectra were recorded at 293 K using a 200, 300, 400 or a 600 MHz spectrometer (Bruker). Shifts (δ) are referenced relative to deuterated solvent residual peaks and expressed in parts per million (ppm). Coupling constants are expressed in hertz (Hz). The following abbreviations are used to explain the observed multiplicities: s (singlet), d (doublet), t (triplet), q (quartet), dd (doublet of doublets), m (multiplet), sbr (broad singlet). High-resolution (HR-ESI-QToF) mass spectra were recorded using a Q-Tof Micromass spectrometer. MALDI-TOF mass spectra were recorded on a Voyager mass spectrometer (Perspective Biosystems, Framingham, MA) equipped with a nitrogen laser. Thin-layer chromatography (TLC) was carried out on aluminum sheets coated with silica gel 60 F_{254} (Merck). TLC plates were inspected by UV light (l = 254 nm) and developed by treatment with a mixture of 10% H_2SO_4 in EtOH/H_2O (1 : 1 v/v), vanillin, $KMnO_4$ or phosphomolybdic acid followed by heating. Silica gel column chromatography was performed with silica gel Si 60 (40–63 mm). Reverse phase chromatography was performed with a C_{18} flash column.

Glycooligonucleotide synthesis

The oligonucleotide synthesis on a solid support was performed on a DNA synthesizer Applied Biosystems (381A or 394A DNA synthesizer). Reactions under microwave activation were performed on a Biotage Initiator system or an Anton Paar Monowave 300 system. Solutions of Cap A, Cap B and iodide were purchased from Link Technologies as well as the commercial solid-supports. Solutions of TCA and CH_3CN for DNA synthesis were purchased from Biosolve. Cy_3-amidite was purchased from GE Healthcare. All glycooligonucleotides were purified and analysed by C_{18} reversed-phase HPLC (Macherey-Nagel, Nucleodur 4.6 × 75 mm, 3 mM) on a Dionex Ultimate 3000 system with a Reodyn injector and a detector UV DAD 3000. Oligonucleotides were dosed by UV-Vis spectrophotometry at 260 nm on a Varian Cary 300 Bio UV-Vis spectrophotometer.

General procedure for N^3-alkylation of uracyls 1 and 2

A solution of propargyl bromide (1.18 eq.) was added to a solution of furanosyl uracil **1** or **2** (1.0 eq.) and potassium carbonate (1.08 eq.) in DMF, and the system was stirred at 60 °C overnight. The reaction mixture was filtered and evaporated to dryness. The crude product was filtered on silica gel column chromatography (5% MeOH in AcOEt) to afford the desired compounds **3a–b**.

1-(β-D-Ribofuranosyl)-3-(prop-2-yn-1-yl)uracil 3a. Obtained as a pale yellow solid (702 mg, 83%) following the general procedure for alkylation: uridine **1** (730 mg, 3.0 mmol), propargyl bromide (420 mg, 3.5 mmol), potassium carbonate (450 mg, 3.2 mmol), DMF (30 mL). ^{1}H NMR (300 MHz, CD_3OD) δ 8.08 (d, J = 8.1 Hz, 1H, H_6), 5.95 (d, J = 4.2 Hz, 1H, $H_{1'}$), 5.82 (d, J = 8.1 Hz, 1H, H_5), 4.68 (dd, J = 2.4, 1.6 Hz, 2H, CH_2C≡CH), 4.22–4.16 (m, 2H, $H_{2'}$, $H_{3'}$), 4.06–4.03 (m, 1H, $H_{4'}$), 3.76–3.92 (dd AB system, J = 9.0, 2.1 Hz, 2H, $H_{5'}$), 2.56 (t, J = 2.4 Hz, 1H, C≡CH). ^{13}C NMR (75 MHz, CD_3OD) δ 163.9, 151.9, 141.3, 102.0, 91.7, 86.4, 79.1, 75.9, 71.9, 71.1, 62.2, 31.1. HR-ESI-QToF MS (positive mode): m/z calcd for $C_{12}H_{15}N_2O_6$ $[M + H]^+$ 283.0930 found 283.0926.

1-(β-D-Arabinofuranosyl)-3-(prop-2-yn-1-yl)uracil 3b. Obtained as a pale yellow solid (761 mg, 90%) following the general procedure for alkylation: arauridine **2** (730 mg, 3.0 mmol), propargyl bromide (420 mg, 3.5 mmol), potassium carbonate (450 mg, 3.2 mmol), DMF (30 mL). ^{1}H NMR (300 MHz, CD_3OD) δ 7.88 (d, J = 8.1 Hz, 1H, H_6), 6.16 (d, J = 4.2 Hz, 1H, $H_{1'}$), 5.76 (d, J = 8.1 Hz, 1H, H_5), 4.66 (dd, J = 2.4, 1.2 Hz, 2H, CH_2C≡CH), 4.19 (dd, J = 4.2, 2.8 Hz, 1H, $H_{2'}$), 4.08 (t, J = 3.3 Hz, 1H, $H_{3'}$), 3.97–3.93 (m, 1H, $H_{4'}$), 3.86–3.76 (dd J_{AB}, J = 11.7, 3.0 Hz, 2H, $H_{5'}$), 2.56 (t, J = 2.4 Hz, 1H, C≡CH). ^{13}C NMR (75 MHz, CD_3OD) δ 162.9, 152.3, 141.5, 95.1, 87.3, 85.4, 77.9, 76.4, 75.8, 70.7, 61.3, 29.8. HR-ESI-QToF MS (positive mode): m/z calcd for $C_{12}H_{15}N_2O_6$ $[M + H]^+$ 283.0930 found 283.0930.

1-(2′,3′,5′-Tri-*O*-acetyl-β-D-xylofuranosyl)uracil 5. Uracil (262 mg, 2.3 mmol, 1.2 eq.) and *N*,*O*-bis(trimethylsilyl)acetamide (1.1 mL, 4.5 mmol, 2.2 eq.) were added to a solution of 1,2,3,5-tetra-*O*-acetyl-D-xylofuranose **4** (637 mg, 2.0 mmol, 1.0 eq.) in CH_3CN (25 mL) and refluxed until the suspension became a clear solution. Then, the reaction mixture was cooled to 0 °C and TMSOTf (511 mg, 2.3 mmol, 1.2 eq.) was

added dropwise, followed by refluxing for 4.5 h. CH_3CN was evaporated under reduced pressure. To the residue was added saturated NH_4Cl solution and the mixture was extracted with CH_2Cl_2. The organic layer was dried with Na_2SO_4, evaporated and nucleoside **5** was purified by silica gel column chromatography (AcOEt : cyclohexane 8 : 2) to afford the title compound **5** (488 mg, 65%). ^{1}H NMR (300 MHz, $CDCl_3$) δ 9.82 (s, 1H, NH), 7.46 (d, J = 8.1 Hz, 1H, H_6), 5.96 (d, J = 2.4 Hz, 1H, $H_{1'}$), 5.74 (d, J = 8.1 Hz, 1H, H_5), 5.30 (dd, J = 3.9, 1.5 Hz, 1H, $H_{3'}$), 5.13 (t, J = 2.1 Hz, 1H, $H_{2'}$), 4.46 (q, J = 9.6, 5.4 Hz, 1H, $H_{4'}$), 4.27 (d, J = 5.7 Hz, 2H, $H_{5'}$). ^{13}C NMR (100 MHz, $CDCl_3$) δ 169.4, 168.1, 168.0, 162.3, 149.3, 138.1, 101.8, 87.4, 78.6, 77.7, 73.3, 59.9, 20.0, 19.7, 19.6. HR-ESI-QToF MS (positive mode): m/z calcd for $C_{15}H_{19}N_2O_9$ $[M + H]^+$ 371.1091 found 371.1092.

1-(β-D-Xylofuranosyl)-3-(prop-2-yn-1-yl)uracil 3c. A solution of propargyl bromide (76 mg, 0.64 mmol, 1.18 eq.) was added to a solution of 2′,3′,5′-tri-*O*-acetyl xylouridine **5** (200 mg, 0.54 mmol, 1.00 eq.) and potassium carbonate (373 mg, 2.7 mmol, 5.00 eq.) in DMF (5 mL). The system was stirred at 60 °C overnight and then methanol was added (300 mL). The reaction mixture was filtered and evaporated to dryness. The crude product was purified by silica gel column chromatography (AcOEt : cyclohexane 8 : 2) to afford the title compound **3c** (98 mg, 65%). ^{1}H NMR (300 MHz, CD_3OD) δ 7.86 (d, J = 8.4 Hz, 1H, H_6), 5.69 (d, J = 3.3 Hz, 1H, $H_{1'}$), 5.67 (d, J = 8.1 Hz, 1H, H_5), 4.55 (d, J = 2.4 Hz, 2H, $CH_2C{\equiv}CH$), 4.22 (m, 1H, $H_{4'}$), 4.04–3.99 (m, 2H, $H_{2'}$, $H_{3'}$), 3.84 (d, J = 5.4 Hz, 2H, $H_{5'}$), 2.45 (t, J = 2.4 Hz, 1H, C≡CH). ^{13}C NMR (75 MHz, CD_3OD): δ 30.87, 61.13, 71.87, 76.42, 79.08, 82.46, 85.49, 94.16, 100.71, 141.72, 151.73, 164.03. HR-ESI-QToF MS (positive mode): m/z calcd for $C_{12}H_{15}N_2O_6$ $[M + H]^+$ 283.0930 found 283.0930.

6-Azido-6-deoxy-D-mannose 9. To a solution of methyl 6-azido-6-deoxy-α-D-mannopyranoside **8**[22] (379 mg, 1.7 mmol, 1 eq.) in H_2O/dioxane (15 mL, 1 : 2) was added a solution of 12 N HCl (4 mL). The mixture was stirred under reflux for 4 h and then a saturated solution of sodium carbonate was added to increase the pH to 7. The crude product was concentrated *in vacuo*, diluted with MeOH and filtered. The filtrate was concentrated and purified by silica gel column chromatography (EtOAc) to afford the desired compound **9** α : β mixture (252 mg, 72%) as a pale yellow oil. Analyses were in agreement with the literature.[41]

6-Azido-6-deoxy-D-mannitol 10. To a solution of 6-azido-6-deoxy-D-mannose **9** (60 mg, 0.29 mmol, 1 eq.) in EtOH (8 mL) was added $NaBH_4$ (66 mg, 1.75 mmol, 6 eq.). The mixture was stirred for 2 h at room temperature and ion exchange resin (DOWEX-50W X8, H^+ form) was then added to decrease the pH to 3. The resin was then removed by filtration. The filtrate was concentrated and co-evaporated with MeOH to give the desired compound **10** after silica gel chromatography (49 mg, 88%). ^{1}H NMR (300 MHz, CD_3OD) δ 3.83–3.61 (m, 5H), 3.55 (dd, J = 12.6, 2.7 Hz, 1H), 3.39 (dd, J = 6.6, 12.6 Hz, 1H). ^{13}C NMR (100 MHz, D_2O) δ 73.0, 71.8, 71.5, 71.0 (4 × *C*HOH), 65.1 (CH_2OH), 55.8 (CH_2N_3). HR-ESI-QToF MS (negative mode): m/z calcd for $C_6H_{12}N_3O_5$ $[M - H]^-$: 206.0777 found 206.0777.

General procedure for elongation of DNA sequences and labelling with Cy3

The DNA sequences were synthesized on the solid-supported scaffolds (LCAA-CPG, 500 Å) at the 1 mmol scale on a DNA synthesizer (ABI 394) by standard phosphoramidite chemistry. For the coupling step, benzylmercaptotetrazole was used as an activator (0.3 M in anhydrous CH_3CN), and commercially available nucleoside phosphoramidites (0.1 M in anhydrous CH_3CN) were introduced with a 20 s coupling time and Cy3 amidite (0.06 M in anhydrous CH_3CN) with a 180 s coupling time. The capping step was performed with acetic anhydride using commercial solution (Cap A, Ac_2O/pyridine/THF, 10 : 10 : 80; Cap B, 10% *N*-methylimidazole in THF) for 15 s. Each oxidation was performed with commercial solution of iodide (0.1 M in THF/pyridine/H_2O, 78 : 20 : 2) for 15 s. Detritylation was performed with 3% TCA in CH_2Cl_2 for 35 s.

Immobilization on solid support 11 or 12 of compounds 3a–c or 10 by CuAAC

An aqueous solution of modified carbohydrates **3a–c** or **10** (0.1 M, 50 mL, 5 eq.), freshly prepared aqueous solutions of $CuSO_4$ (0.1 M, 4 mL, 0.4 eq.) and sodium ascorbate (0.5 M, 4 mL, 2 eq.), TEAAc buffer (50 mL), water (17 mL) and MeOH (125 mL) were added to 1 mmol of solid support **11** or **12**. The resulting mixture was heated at 65 °C for 1 h. The solution was removed, and CPG beads were washed with H_2O (3 × 2 mL), MeOH (3 × 2 mL) and CH_3CN (3 × 2 mL), and dried.

General procedure for introduction of phosphoramidites 13–15 on furanoside and reduced mannoside scaffolds

Solid-supported furanoside **18a–c** and mannitol **28** scaffolds (1 mmol) were treated by phosphoramidite chemistry, on a DNA synthesizer, with phosphoramidites **13**, **14** or **15**. Only coupling and oxidation steps were performed. For the coupling step, benzylmercaptotetrazole was used as an activator (0.3 M in anhydrous CH_3CN) and phosphoramidites **13–15** (0.3 M with the platform **18a–c** and 0.5 M with the platform **28** in anhydrous CH_3CN) were introduced three times with a 180 s coupling time. Oxidation was performed with 0.1 M commercial solution of iodide for 15 s.

General procedure for deprotection of solid-supported alkyne oligonucleotides

The CPG beads bearing modified oligonucleotides were transferred to a 4 mL screw top vial and treated with 2 mL of concentrated aqueous ammonia for 15 h at room temperature and warmed to 55 °C for 2 h. The supernatants were withdrawn and evaporated.

General procedure for introduction of galactoside 16 or fucoside 17 derivatives by CuAAC reaction

In solution. To a solution of 5′-fluorescent-3′-alkyne oligonucleotides **21a–c** and **22a–c** (100 nmol) were added galactoside **16** or fucoside **17** derivatives (3 eq. per alkyne function, 0.1 M in MeOH or dioxane for **16**), 1 mg of $Cu^{(0)}$ nanopowder,

0.1 M triethylammonium acetate buffer, pH 7.7 (25 mL), water and MeOH or dioxane to obtain a final volume of 250 mL (water/MeOH, 1 : 1 v/v). The resulting mixture was heated at 65 °C for 1 h. EDTA (0.1 M, 100 mL) was added to the mixtures, and after centrifugation, the supernatants were withdrawn to eliminate Cu(0) and desalted by size exclusion chromatography on NAP10. After evaporation, the 5′-fluorescent 3′-acetyl-glycomimetic oligonucleotides were treated with concentrated aqueous ammonia for 2 h at room temperature to remove acetyl groups and evaporated. Final compounds were purified by C_{18} reversed phase HPLC.

On solid support. A solution of galactoside **16** or fucoside **17** derivatives (5 eq. per alkyne function, 0.1 M in MeOH or dioxane for **16**), freshly prepared aqueous solutions of $CuSO_4$ (0.1 M, 0.4 eq.) and sodium ascorbate (0.5 M, 2 eq.), and TEAAC buffer (50 mL) were added to the solid supported oligonucleotides **29a–c** (1 mmol). The resulting mixture was heated at 70 °C for 1 h. The solution was removed, and CPG beads were washed with H_2O (3 × 2 mL), MeOH (3 × 2 mL) and CH_3CN (3 × 2 mL), and dried. Finally, the DNA sequence was elongated and labelled with Cy3.

Microarray production and K_d microarray assays

The procedure has been described by Goudot *et al.*[25] 3′-Amino-modified oligonucleotides were purchased from Eurogentec and chemicals from Sigma-Aldrich. An Alexa Fluor® 647 Microscale Protein Labelling Kit was purchased from Invitrogen. Fluorescence scanning was performed using an Axon microarray scanner, and the GenePix 4100A software package.

Microarray production. Nexterion Glass D slides from Schott AG were used. The slides were structured by adapting the protocol of Mazurczyk *et al.*[42] leading to slides bearing 40 microwells (square 3 × 3 mm, depth: 102 ± 1 μm, with 4.5 mm spacing between each well).

The resulting glass slides were silanized according to the gas phase protocol[43] leading to a *tert*-butyl ester functionalized surface. Deprotection of the acid function was accomplished in glacial formic acid for 7 h. The slides were washed in dichloromethane and water (10 min, under ultrasound). Activation of the carboxylic function was performed using diisopropylcarbodiimide and *N*-hydroxysuccinimide solution at 0.1 M in tetrahydrofuran, overnight at room temperature. The slides were washed in THF followed by dichloromethane (10 min, ultrasounds).

Next, four amino-modified oligonucleotides (25 μM, PBS 10× pH 8.5) were covalently immobilized in an array fashion using a Scienion sciFLEXARRAYER s3 system piezoelectric. Amino-modified oligonucleotides were spotted at 25 μM for LecB and at 0.5 μM for LecA and BambL in 10× PBS (pH 8.5). The immobilized sequences were 5′-GTG AGC CCA GAG GCA GGG-$(CH_2)_7$-NH_2, 5′-GTG GAG GCA CCA AGC TTT-$(CH_2)_7$-NH_2, 5′-CCA AGC GAG GTG GCA TTT-$(CH_2)_7$-NH_2 and 5′-CCA GCA GTG GAG AGC TTT-$(CH_2)_7$-NH_2. In each microwell, 64 spots of two sequences (2 × 32 spots) were spotted under a water saturated atmosphere. Water was allowed to evaporate gently overnight. Then, slides were washed for 30 min at 70 °C in 0.1% SDS and rinsed with water.

Blocking non-specific adsorption was performed using Bovine Serum Albumin (BSA). This step was performed before DDI of the glycoclusters and repeated before incubation with the lectins. The slides were incubated with a 4% BSA solution; in 1× PBS, pH 7.4 for 2 h. The slides were washed in 1× 0.05% PBS-Tween20 (3 × 3 min), in 1× PBS (3 × 3 min) and rinsed with water.

Immobilization of the glycoclusters was accomplished using DNA directed Immobilization (DDI).[26] Two μL of a mixture containing two different glycoclusters (1 μM per glycocluster in 1× PBS pH 7.4) was poured at the bottom of each microwell and incubated (3 h, 37 °C, in a water saturated chamber). The slides were washed in 2× SSC , 0.1% SDS at 51 °C for 1 min, 2× SSC for 5 min and rinsed with water. Correct immobilization of the Cy3 labeled glycoclusters was ensured by scanning the slides at 532 nm (excitation of Cy3). The fluorescence signal of each glycocluster was determined as the average of the mean fluorescence signal of 32 spots. The surface densities of the glycoclusters deviated by less than 14%.

Lectins LecA, LecB and BambL (a gift from Dr Anne Imberty, CERMAV) were labeled with Alexa 647 according to the supplier protocol. The degrees of labeling per lectin (multimeric form) were 0.30, 0.34 and 0.24 moles of Alexa-647 per mole of lectin respectively.

K_d determination. Solutions of 2% BSA, 7.5 μM $CaCl_2$ and labeled lectin ranking from 0.01 nM to 2.0 μM for LecA and BambL (or 1 nM to 2.4 μM for LecB) were prepared in 1× PBS (pH 7.4) in order to draw isotherm curves of 20 discrete points. In each microwell, 2 μL of solution was added and incubated for 3 h at 37 °C in a water saturated chamber. Then, slides were washed for 5 min with 1× 0.02% PBS-Tween20 and rinsed with water. An average of 32 spots per glycocluster of the mean fluorescence signal at 635 nm (FI) was calculated. For each glycocluster, K_d values were determined by the intercept with the *y*-axis using the linear regression: $[LecA]/FI = 1/FI_{max} \times [LecA] + K_d/FI_{max}$.

In silico molecular docking

The three dimensional structures of LecA and LecB were retrieved from the Protein Data Bank (http://www.rcsb.org) under the PDB codes 2VXJ and 1UVZ respectively. As an example, the building procedure of the lectin (LecA)–ligand (**G2b**) complex is depicted as follows: the galactose endings of the two glycocluster branches linked on C2 and C3 of the arabinofuranose ring are brought close to the crystallographic galactose ligands (Fig. S1†). The terminal sugars of the two glycocluster branches are removed and the chemical bond with the galactose moieties of LecA is built (Fig. S2†). LecA and its two galactose groups are considered as aggregates and the complex is optimized (Fig. S2†). A classical Monte Carlo conformational searching procedure is then performed as described using the BOSS software.[44] The constraints have been removed and the whole structure was relaxed. In the

minimization procedures, the spectroscopic empirical energy function SPASIBA and the corresponding parameters are used.[45–47] A typical lowest energy structure for the complex LecA–**G2b** is shown in Fig. S3.†

In the same way, an empirical potential energy of interaction ΔE for the lectin–ligand complexes using the simple expression:

$$\Delta E_{\text{interaction}} = E_{\text{complex}} - E_{\text{protein}} - E_{\text{ligand}}$$

was evaluated using the same force field.

Acknowledgements

This work was financially supported by ANR-12-BSV5-0020 "GLYCOMIME". Plateforme NanoLyon is acknowledged for its technical support. C. L and A. A. thank the University of Montpellier for a research studentship. F.M. is a member of Inserm.

References

1 N. Gilboa-Garber, *Methods Enzymol.*, 1982, **83**, 378–385.
2 A. Imberty, M. Wimmerova, E. P. Mitchell and N. Gilboa-Garber, *Microbes Infect.*, 2004, **6**, 221–228.
3 D. Sicard, S. Cecioni, M. Iazykov, Y. Chevolot, S. E. Matthews, J. P. Praly, E. Souteyrand, A. Imberty, S. Vidal and M. Phaner-Goutorbe, *Chem. Commun.*, 2011, **47**, 9483–9485.
4 S. Cecioni, R. Lalor, B. Blanchard, J. P. Praly, A. Imberty, S. E. Matthews and S. Vidal, *Chem. – Eur. J.*, 2009, **15**, 13232–13240.
5 S. Cecioni, A. Imberty and S. Vidal, *Chem. Rev.*, 2015, **115**, 525–561.
6 K. Buffet, E. Gillon, M. Holler, J. F. Nierengarten, A. Imberty and S. P. Vincent, *Org. Biomol. Chem.*, 2015, **13**, 6482–6492.
7 A. Audfray, J. Claudinon, S. Abounit, N. Ruvoen-Clouet, G. Larson, D. F. Smith, M. Wimmerova, J. Le Pendu, W. Romer, A. Varrot and A. Imberty, *J. Biol. Chem.*, 2012, **287**, 4335–4347.
8 C. Ligeour, A. Audfray, E. Gillon, A. Meyer, N. Galanos, S. Vidal, J. J. Vasseur, A. Imberty and F. Morvan, *RSC Adv.*, 2013, **3**, 19515–19524.
9 B. Richichi, A. Imberty, E. Gillon, R. Bosco, I. Sutkeviciute, F. Fieschi and C. Nativi, *Org. Biomol. Chem.*, 2013, **11**, 4086–4094.
10 R. J. Pieters, *Org. Biomol. Chem.*, 2009, **7**, 2013–2025.
11 G. Pourceau, A. Meyer, Y. Chevolot, E. Souteyrand, J. J. Vasseur and F. Morvan, *Bioconjugate Chem.*, 2010, **21**, 1520–1529.
12 B. Gerland, A. Goudot, G. Pourceau, A. Meyer, V. Dugas, S. Cecioni, S. Vidal, E. Souteyrand, J. J. Vasseur, Y. Chevolot and F. Morvan, *Bioconjugate Chem.*, 2012, **23**, 1534–1547.
13 B. Gerland, A. Goudot, C. Ligeour, G. Pourceau, A. Meyer, S. Vidal, T. Gehin, O. Vidal, E. Souteyrand, J. J. Vasseur, Y. Chevolot and F. Morvan, *Bioconjugate Chem.*, 2014, **25**, 379–392.
14 B. Gerland, A. Goudot, G. Pourceau, A. Meyer, S. Vidal, E. Souteyrand, J.-J. Vasseur, Y. Chevolot and F. Morvan, *J. Org. Chem.*, 2012, **77**, 7620–7626.
15 G. Pourceau, A. Meyer, J. J. Vasseur and F. Morvan, *J. Org. Chem.*, 2009, **74**, 6837–6842.
16 J. Lietard, A. Meyer, J. J. Vasseur and F. Morvan, *J. Org. Chem.*, 2008, **73**, 191–200.
17 C. Ligeour, A. Meyer, J. J. Vasseur and F. Morvan, *Eur. J. Org. Chem.*, 2012, 1851–1856.
18 S. Cecioni, J. P. Praly, S. E. Matthews, M. Wimmerova, A. Imberty and S. Vidal, *Chem. – Eur. J.*, 2012, **18**, 6250–6263.
19 F. Morvan, A. Meyer, A. Jochum, C. Sabin, Y. Chevolot, A. Imberty, J. P. Praly, J. J. Vasseur, E. Souteyrand and S. Vidal, *Bioconjugate Chem.*, 2007, **18**, 1637–1643.
20 M. Nakane, S. Ichikawa and A. Matsuda, *J. Org. Chem.*, 2008, **73**, 1842–1851.
21 B. R. Baker, in *The Ciba Foundation Symposium on the Chemistry and Biology of the Purine*, ed. G. E. W. Wolstenholme and C. M. O'Connor, John Wiley & Sons, Chichester, UK, 1957, pp. 120–133.
22 J. J. Reina, O. S. Maldonado, G. Tabarani, F. Fieschi and J. Rojo, *Bioconjugate Chem.*, 2007, **18**, 963–969.
23 L. Chaveriat, I. Stasik, G. Demailly and D. Beaupere, *Tetrahedron: Asymmetry*, 2006, **17**, 1349–1354.
24 Since the catalytic form of copper is Cu(I), Cu(0) was used as a nanopowder to ensure a large specific surface area allowing its oxidation by oxygen contained in solvents.
25 A. Goudot, G. Pourceau, A. Meyer, T. Gehin, S. Vidal, J. J. Vasseur, F. Morvan, E. Souteyrand and Y. Chevolot, *Biosens. Bioelectron.*, 2013, **40**, 153–160.
26 Y. Chevolot, C. Bouillon, S. Vidal, F. Morvan, A. Meyer, J. P. Cloarec, A. Jochum, J. P. Praly, J. J. Vasseur and E. Souteyrand, *Angew. Chem., Int. Ed.*, 2007, **46**, 2398–2402.
27 R. Wacker and C. M. Niemeyer, *ChemBioChem*, 2004, **5**, 453–459.
28 J. Zhang, G. Pourceau, A. Meyer, S. Vidal, J.-P. Praly, E. Souteyrand, J.-J. Vasseur, F. Morvan and Y. Chevolot, *Biosens. Bioelectron.*, 2009, **24**, 2515–2521.
29 J. Zhang, G. Pourceau, A. Meyer, S. Vidal, J. P. Praly, E. Souteyrand, J. J. Vasseur, F. Morvan and Y. Chevolot, *Chem. Commun.*, 2009, 6795–6797.
30 S. Park and I. Shin, *Org. Lett.*, 2007, **9**, 1675–1678.
31 F. Pertici, N. J. de Mol, J. Kemmink and R. J. Pieters, *Chem. – Eur. J.*, 2013, **19**, 16923–16927.
32 F. Casoni, L. Dupin, G. Vergoten, A. Meyer, C. Ligeour, T. Gehin, O. Vidal, E. Souteyrand, J. J. Vasseur, Y. Chevolot and F. Morvan, *Org. Biomol. Chem.*, 2014, **12**, 9166–9179.
33 N. Garber, U. Guempel, A. Belz, N. Gilboa-Garber and R. J. Doyle, *Biochim. Biophys. Acta*, 1992, **1116**, 331–333.
34 R. U. Kadam, M. Bergmann, M. Hurley, D. Garg, M. Cacciarini, M. A. Swiderska, C. Nativi, M. Sattler,

A. R. Smyth, P. Williams, M. Camara, A. Stocker, T. Darbre and J. L. Reymond, *Angew. Chem., Int. Ed.*, 2011, **50**, 10631–10635.

35 J. Rodrigue, G. Ganne, B. Blanchard, C. Saucier, D. Giguere, T. C. Shiao, A. Varrot, A. Imberty and R. Roy, *Org. Biomol. Chem.*, 2013, **11**, 6906–6918.

36 R. U. Kadam, D. Garg, J. Schwartz, R. Visini, M. Sattler, A. Stocker, T. Darbre and J. L. Reymond, *ACS Chem. Biol.*, 2013, **8**, 1925–1930.

37 M. L. Gening, D. V. Titov, S. Cecioni, A. Audfray, A. G. Gerbst, Y. E. Tsvetkov, V. B. Krylov, A. Imberty, N. E. Nifantiev and S. Vidal, *Chem. – Eur. J.*, 2013, **19**, 9272–9285.

38 C. Ligeour, L. Dupin, A. Marra, G. Vergoten, A. Meyer, A. Dondoni, E. Souteyrand, J. J. Vasseur, Y. Chevolot and F. Morvan, *Eur. J. Org. Chem.*, 2014, 7621–7630.

39 J. J. P. Stewart, *J. Mol. Model*, 2007, **13**, 1173–1213.

40 G. D. Hawkins, C. J. Cramer and D. G. Truhlar, *J. Phys. Chem.*, 1996, **100**, 19824–19839.

41 D. C. M. Kong and M. von Itzstein, *Carbohydr. Res.*, 1997, **305**, 323–329.

42 R. Mazurczyk, G. E. Khoury, V. Dugas, B. Hannes, E. Laurenceau, M. Cabrera, S. Krawczyk, E. Souteyrand, J. P. Cloarec and Y. Chevolot, *Sens. Actuators, B*, 2008, **128**, 552–559.

43 M. Phaner-Goutorbe, V. Dugas, Y. Chevolot and E. Souteyrand, *Mater. Sci. Eng., C*, 2011, **31**, 384–390.

44 W. L. Jorgensen and J. Tirado-Rives, *J. Comput. Chem.*, 2005, **26**, 1689–1700.

45 P. Derreumaux and G. Vergoten, *J. Chem. Phys.*, 1995, **102**, 8586–8605.

46 G. Vergoten, I. Mazur, P. Lagant, J. C. Michalski and J. P. Zanetta, *Biochimie*, 2003, **85**, 65–73.

47 P. Lagant, D. Nolde, R. Stote, G. Vergoten and M. Karplus, *J. Phys. Chem. A*, 2004, **108**, 4019–4029.